Supporting Information

Jackson et al. 10.1073/pnas.1417456111

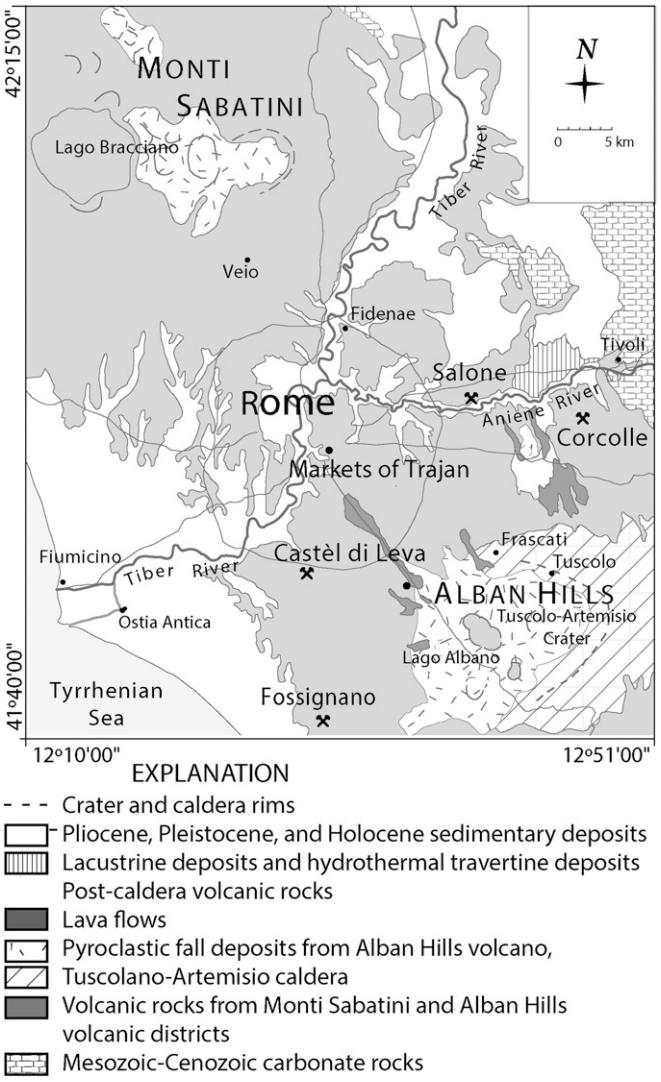

Fig. S1. Geologic sketch map of the Roman region, showing the Pozzolane Rosse quarries at Castel di Leva, Corcolle and Fossignano and Tufo Lionato quarry at Salone (after ref. 1).

1. Jackson MD, Deocampo D, Marra F, Scheetz B (2010) Mid-Pleistocene volcanic ash in ancient Roman concretes. *Geoarchaeology* 25(1):36–74.

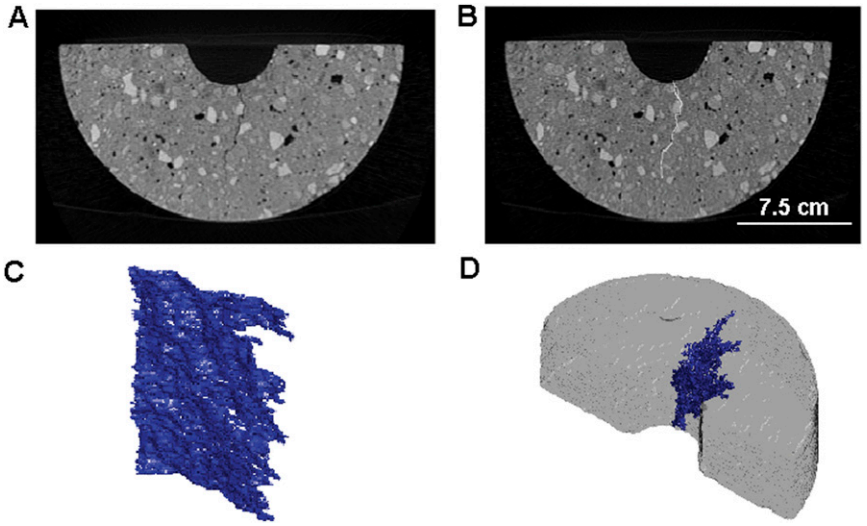

Fig. S2. Illustration of method used to determine the experimental fracture energy (G_f) from tomographic measurements. The work of fracture is obtained from the integrated load vs. load-line displacement curve and then normalized by the traced area of the tomographic fracture surfaces (Table S2). (*A*) Typical tomographic slice of a fractured specimen with the crack traced in (*B*). (*C*) Three-dimensional rendering of the complete traced crack array and (*D*) distribution of cracks in the arc-shaped mortar specimen.

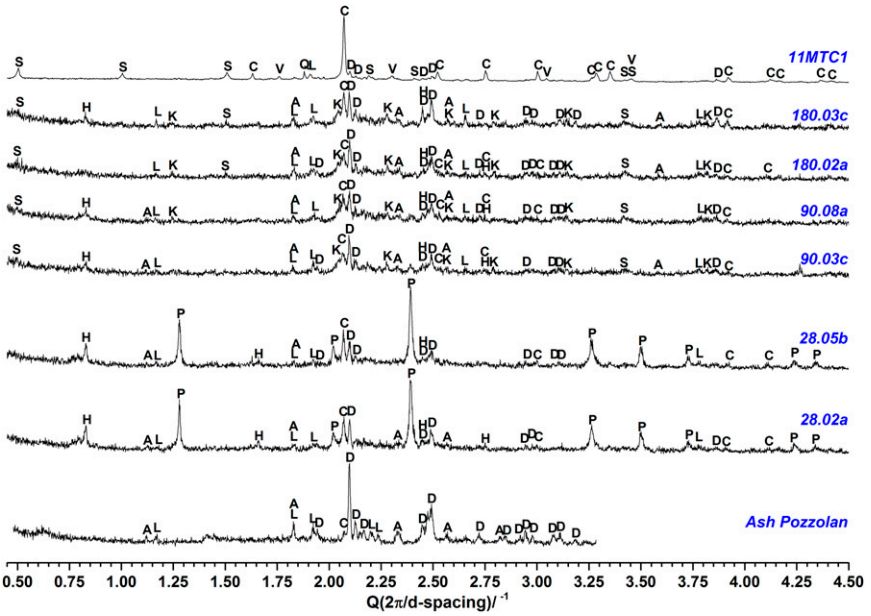

Fig. S3. Powder X-ray diffraction analyses of the cementitious matrix (<74 μm) gently tapped and hand-shaken through sieves to <200 mesh from the mortar reproduction at 28, 90, and 180 d of hydration, the 11MTC1 mortar from the foundation of the Markets of Trajan at Via Biberati and the ash pozzolan mix, using a Scintag PADV X-ray diffractometer, equipped with a Ge solid state detector and Cu–Ka radiation, 35 kV/30 mA, at the Materials Characterization Laboratory at Pennsylvania State University. For bulk chemical analyses as weight percent oxides see Table S5.

Table S1. Grain size distribution of Pozzolane Rosse ash from Castel di Leva quarry (Fig. S1), expressed as weight percent retained on sieves

	Gravel (lapilli)		Sand (ash)					Silt
ASTM sieve no.	4	8	16	30	50	100	200	PAN
Weight %	26.7	18.75	15.34	10.8	9.66	9.66	6.25	2.84
Opening size, mm	4.75	2.38	1.2	0.6	0.3	0.15	0.08	<0.075

Determined through the ASTM C36-06 Standard Test Method for Sieve Analysis of Fine and Coarse Aggregates (after ref. 1).

1. Jackson MD, et al. (2007) Geological observations of excavated sand (*harenae fossiciae*) used as fine aggregate in ancient Roman pozzolanic mortars. *J Roman Arch* 20:1–30.

Table S2. Measurements of fracture surface area in the mortar reproductions (Fig. 4)

Tomographic analysis			Experimental testing data		
Crack surfaces,* voxels	Voxel face area, mm^2	Traced crack area,† mm^2	Work of fracture (from load-loadline displacement), mJ	Experimental fracture energy (G_f), J/m^2	Peak load (P_{max}), N
113,000	0.21	11,770.01	44	4	345
85,000	0.20	8,320.96	45	5	298
120,000	0.20	11,898.16	47	4	336
67,000	0.19	6,367.54	33	5	277
120,000	0.20	11,434.29	40	3	337
110,000	0.22	12,407.43	42	3	355
—	—	—	52	—	345
—	—	—	66	—	376
55,000	0.31	8,555.95	297	35	1,986
57,000	0.30	8,579.21	319	37	1,705
50,000	0.33	8,000.67	296	37	1,740
33,000	0.31	5,154.65	342	66	2,201
44,000	0.30	6,612.96	341	52	1,833
40,000	0.20	5,890.61	263	45	1,722
44,000	0.30	6,824.25	354	52	1,703
30,000	0.30	4,767.35	299	63	1,676

Measured from computed tomography scans performed at the Cornell University Hospital for Animals, at "bone density" setting with a slice spacing of 0.5 mm, and ImageJ tracings of all apparent crack surfaces in the ~75 slices of each specimen. A crack area algorithm summed the voxels (3D pixels) of these surfaces. Dashes indicate that high-resolution scans are not available for these samples.

*Error is <5% based on tracings by as many as three different individuals.

†The traced area is the average of both walls of the cracks.

Table S3. Characteristic d-spacings of minerals identified through X-ray microdiffraction analysis (Fig. 3)

Crystallographic parameters			X-ray microdiffraction analysis		
d-spacing, Å	Intensity, %	(hkl)	180d CM Pt 11 (Fig. 3*A*)	MT CM Pt 10 (Fig. 3*C*)	MT SCOR1 Pt 18 (Fig. 3*E*)
12.59	100	0 0 3	12.62	12.40	12.51
4.20	56	0 0 9	4.22		4.20
2.87	44	1 1 0	2.87	2.87	2.87
6.30	31	0 0 6	6.29	6.27	6.30
2.61	23	1 1 6	2.61	2.61	2.61
4.16	21	1 0 5	4.16	4.17	
1.89	17	1 1 15		1.88	
		2 0 13			
1.83	16	2 0 14		1.83	1.83
4.40	15	1 0 4	4.40		4.40
2.41	14	2 0 4	2.41	2.41	
4.93	13	1 0 1		4.93	
2.03	11	1 0 17	2.02	2.02	2.02
2.12	11	1 1 12	2.12	2.12	2.12
2.37	11	1 1 9		2.37	2.37
2.51	8	1 0 13	2.51		
3.42	8	1 0 8	3.44		
2.01	6	2 0 11	2.00		2.00
	Åkermanite			MT SCOR1 Pt 18 (Fig. 3*E*)	
2.87	100	2 1 1		2.87	
3.09	23	2 0 1		3.08	
1.76	22	3 1 2		1.77	
2.48	16	3 1 0		2.49	
1.85	12	3 3 0		1.84	
1.78	11	4 1 1		1.77	
	Katoite		180d CM Pt 11 (Fig. 3*A*)		MT SCOR1 Pt 18 (Fig. 3*E*)
2.77	100	4 2 0	2.77		2.76
2.01	91	1 1 6	2.00		2.00
2.26	79	5 2 1	2.27		2.25
1.65	70	6 4 2			1.65
5.05	53	1 1 2	5.05		
3.10	52	4 0 0	3.11		
1.72	48	6 4 0			1.71
2.43	31	4 3 1	2.43		
3.31	28	3 2 1	3.33		
2.53	18	2 2 4	2.53		

Analyzed at beamline 12.3.2 of the Advanced Light Source at Lawrence Berkeley National Laboratory. A monochromatic X-ray beam of 10 keV was focused to 2- (v) × 8- (h) μm diameter on a thin (0.3-mm) slice of mortar placed in transmission mode into the beam, with the detector 2θ at 39° for the 11MTC1 sample and at 360° for the 180-02 sample. A Pilatus 1M area detector placed at 360 mm recorded Debye rings diffracted by crystalline phases that were radially integrated into intensity vs. 2θ plots over an arch segment of 76° for 2θ 3°–30°.

Table S4. Compositions of cementitious hydrates determined through SEM-EDS analyses from the 28-d (28-05), 180-d (180-02), and 1,900-y Great Hall (GRAULA20-A) mortars (Fig. 2)

Mortar, atomic %	Ca	Al	Si	Al/(Si+Al)	Ca/(Si+Al)	Ca/Si
28-d cementitious matrix						
C-A-S-H						
3.2	20.37	26.05	53.58	0.33	0.26	0.38
1.5	52.23	10.01	37.76	0.21	1.09	1.38
1.6	54.06	7.89	38.06	0.17	1.18	1.42
3.4	75.81	7.74	16.45	0.32	3.13	4.61
3.5	76.71	5.24	18.05	0.22	3.29	4.25
Fiber						
1.2	58.87	37.65	3.47	0.92	1.43	16.96
3.6	59.56	34.48	5.96	0.85	1.47	10.00
1.3	59.57	32.92	7.50	0.81	1.47	7.94
C-S-H and opal						
1.7	11.01	9.02	79.97	0.10	0.12	0.14
3.7	0.00	0.00	100.00	0.00	0.00	0.00
3.8	62.07	0.00	37.93	0.00	1.64	1.64
180-d cementitious matrix						
C-A-S-H						
4.4	47.14	10.55	42.32	0.20	0.89	1.11
4.5	47.01	14.66	38.34	0.28	0.89	1.23
5.3	46.37	12.18	41.45	0.23	0.86	1.12
5.4	47.88	17.07	35.05	0.33	0.92	1.37
3.3	41.63	14.57	43.80	0.25	0.71	0.95
1.3	44.05	13.38	42.57	0.24	0.79	1.03
15	53.51	11.95	34.54	0.26	1.15	1.55
16	45.10	11.73	43.17	0.21	0.82	1.04
17	46.63	10.22	43.15	0.19	0.87	1.08
18	46.97	11.29	41.74	0.21	0.89	1.13
19	48.48	9.29	42.23	0.18	0.94	1.15
Plate/fiber						
2.1	48.39	31.09	20.52	0.60	0.94	2.36
2.2	45.98	33.68	20.34	0.62	0.85	2.26
4.1	60.01	34.57	5.42	0.86	1.50	11.08
4.3	53.32	27.12	19.57	0.58	1.14	2.72
6.4	59.73	38.18	2.10	0.95	1.48	28.46
Al-rich C-A-S-H						
3.1	52.75	38.51	8.74	0.81	1.12	6.03
4.2	52.33	38.08	9.59	0.80	1.10	5.45
5.1	54.34	36.96	8.70	0.81	1.19	6.24
5.2	52.22	39.81	7.96	0.83	1.09	6.56
6.1	45.13	38.18	16.69	0.70	0.82	2.70
6.2	44.42	26.76	28.82	0.48	0.80	1.54
6.3	46.13	30.28	23.58	0.56	0.86	1.96
6.5	44.78	33.52	21.70	0.61	0.81	2.06
Great Hall, cementitious matrix						
C-A-S-H						
1	59.68	24.10	16.23	0.60	1.48	3.68
2	42.76	34.36	22.88	0.60	0.75	1.87
3	40.82	33.15	26.03	0.56	0.69	1.57
5	32.23	38.34	29.43	0.57	0.48	1.10
7	31.81	38.32	29.86	0.56	0.47	1.07
14	40.46	32.90	26.64	0.55	0.68	1.52
17	24.64	41.76	33.60	0.55	0.33	0.73
18	31.70	31.86	36.44	0.47	0.46	0.87

Analyzed using a Zeiss EVOMA10 scanning electron microscope at the Department of Earth and Planetary Science at the University of California, Berkeley. Operating conditions were a beam energy of 15 keV, beam current of 850 pA, and counting time of 10 s with 3,500 counts per second for EDS analyses. Counts were converted to semiquantitative concentrations and atomic ratios for Ca, Si, and Al.

Table S5. Major element compositions as weight percent oxides of the <74 μm fraction (passing the 200 sieve) of the ash pozzolan and mortars

Sample	SiO_2	Al_2O_3	Fe_2O_3(T)	MnO	MgO	CaO	Na_2O	K_2O	TiO_2	P_2O_5	LOI	Total
Ash Pozzolan												
01	43.48	16.58	9.46	0.18	3.72	10.10	0.80	2.45	0.80	0.67	10.90	99.14
02	43.80	16.73	9.40	0.18	3.73	9.89	0.82	2.50	0.80	0.65	11.23	99.72
28 d												
28.02a	19.76	8.00	3.98	0.09	1.90	32.28	0.32	1.15	0.34	0.27	28.50	96.57
28.05b	18.08	7.43	3.56	0.08	1.73	33.31	0.28	0.97	0.30	0.22	30.94	96.89
28.05c	20.06	8.08	3.96	0.09	1.88	31.18	0.33	1.18	0.34	0.25	27.11	94.46
90 d												
90.08a	22.35	8.71	4.42	0.09	2.00	23.88	0.34	1.17	0.38	0.29	30.98	94.61
90.08b	22.46	8.91	4.26	0.09	1.94	24.71	0.32	1.13	0.36	0.27	31.23	95.70
90.03c	21.83	8.49	4.23	0.09	1.92	24.71	0.30	1.14	0.36	0.28	33.95	97.29
180 d												
180.02a	23.07	9.07	4.34	0.10	1.97	22.94	0.33	1.22	0.37	0.30	33.33	97.02
180.02b	21.74	8.62	4.04	0.09	1.80	21.46	0.33	1.14	0.34	0.26	36.80	96.63
180.03c	22.44	9.02	4.25	0.09	1.90	23.10	0.31	1.16	0.36	0.27	36.42	99.32
1,900 y												
11MTC1	24.49	9.43	2.65	0.06	1.53	28.14	0.61	0.98	0.24	0.22	30.69	99.04

The compositions of the Trajanic volcanic ash mix, mortar reproduction at 28, 90, and 180 d of hydration and the 11MTC1 mortar specimen from the foundation of the Markets of Trajan at Via Biberati (Fig. 2*E*), were determined through lithium metaborate/tetraborate fusion with high-resolution inductively coupled plasma mass spectrometry, at Activation Laboratories, Ontario, Canada. For X-ray powder diffraction studies see Fig. S3.